Astron. Astrophys. 349, 135–150 (1999)

ASTRONOMY AND ASTROPHYSICS

Nuclear properties in early stages of stellar collapse

F.K. Sutaria[1], **A. Ray**[2,3], **J.A. Sheikh**[2,4], **and P. Ring**[4]

[1] Inter University Center for Astronomy and Astrophysics, Pune 411 007, India
[2] Tata Institute of Fundamental Research, Mumbai 400 005, India
[3] Lab for High Energy Astrophysics, NASA/Goddard Space Flight Center, Greenbelt, MD 20771, USA
[4] Physik-Department, Technische Universitat München, D-85747 Garching, Germany

Received 31 July 1998 / Accepted 13 April 1999

Abstract. The spectroscopy of electron capture neutrinos emitted from nearby pre-supernova collapsing stars before the neutrino trapping sets in, can yield useful information on the physical conditions and on the nuclear composition of the core. The neutrino spectrum depends on the thermodynamic conditions of the core, the nuclear abundances, the lepton fractions and relevant nuclear properties. In the pre-trapping core, the density ranges from 0.1–$100\ 10^{10}$ g/cm^3 and the temperature from 0.2–1.5 MeV. The nuclear abundances can be obtained under the assumption of Nuclear Statistical Equilibrium (NSE). The nuclear abundances as well as the electron capture rates are thus determined, among other things, by the nuclear binding energies and the free nucleon chemical potentials. Because shell and pairing effects persist strongly up to temperatures of $\simeq 0.5$ MeV, any equation of state (EOS) relevant to this phase of the collapse must reproduce well the zero temperature nuclear properties and it must show a smooth transition to the known high temperature and high density limits. In this work we use the microscopic Relativistic Mean Field (RMF) theory based on a Lagrangian with non-linear self-interactions of the σ-field for the neutron-rich nuclei of interest in the $f-p$ shell to determine nuclear chemical potentials. We compare these results with those computed from an EOS calculated with the macroscopic liquid drop model. We also discuss extensions to finite temperature and we incorporate nuclear lattice effects into the microscopic calculations.

Key words: stars: supernovae: general – equation of state – nuclear reactions, nucleosynthesis, abundances

1. Introduction

The collapse of the core of a massive star is believed to lead to the explosion of a type II supernova. So far, however, numerical simulations of such a collapse have not been able to demonstrate convincingly the explosions observed in nature. Such simulations require many detailed and complex physical inputs, such as the equation of state of dense and warm stellar matter, the hydrodynamics of the shock wave, or the energy transport by neutrinos. The calculation of the equation of state of the stellar core material at densities below the nuclear saturation densities ($10^9 < \rho < 10^{13}$ g/cm^3) constitutes, technically, one of the most computer intensive parts, because it requires a high accuracy due to its influence on the early part of the supernova development (see e.g. Cooperstein & Baron 1990).

Initially, at densities of 10^9 g/cm^3 the core is composed of heavy nuclei immersed in a electrically neutral plasma of electrons, with a small fraction of drip neutrons and an even smaller fraction of drip protons. Nevertheless, the overall density being much lower than nuclear matter density, the average volume available to a single nucleus is much greater than that of the nuclear volume. Under such circumstances the equation of state can be approximated by that of a Boltzmann gas of heavy nuclei, and drip particles in Nuclear Statistical Equilibrium (NSE), together with a highly degenerate, electrically neutralizing gas of non-interacting electrons. This state of affairs persists up to densities of $\sim 10^{12}\ \mathrm{g/cm^3}$, where the ratio of the nuclear radius ($R_N \sim A^{1/3}$) to the Coulomb interaction radius ($R_c \sim (A/\rho)^{1/3}$) given by $R_N/R_c \simeq 10^5\rho^{1/3}$ is no longer small $\ll 1$ and the nuclei start interacting with each other by means of Coulomb lattice effects. Finally, at values around $10^{13}\ \mathrm{g/cm^3}$ the density of the "vapor" of free nucleons surrounding the droplets of nuclear matter is too high to justify the treatment of nuclei as a Boltzmann gas of *non-interacting* particles (see e.g. Hillebrandt (1994) and references therein).

The equation of state of moderately neutron-rich matter at intermediate temperature and density can substantially influence the energy spectrum and the flux of the early phase neutrinos from electron capture on nuclei and free protons. Should the neutrinos from the collapse phase be detected from a nearby supernova in an underground neutrino detection experiment such as the Sudbury Neutrino Observatory (SNO) or the Super-Kamioka (SK), such spectra could be possibly measured. This will be possible only under the assumptions, that such a supernova explosion will occur at a distance of approximately 1 kpc and that these new generation of neutrino detectors with increased sensitivity are available at that time (see Sutaria & Ray (1997), hereafter SR). The neutrinos from the early phase of the

Send offprint requests to: A. Ray (akr@tifr.res.in)
Correspondence to: Tata Institute of Fundamental Research, Mumbai 400 005, India

collapse, before they are trapped by dense overlying matter are especially interesting for several reasons. They bear information directly related to the conditions under which they are produced (SR). The pre-trapping phase of the emission of core-neutrinos continues until the overlying density grows to about 10^{12} g/cm^3. The emitted neutrino spectrum depends upon the individual Q-values Q_i of the nuclei involved in the electron-capture reaction. Both these Q-values as well as the overall abundance of particular nuclei depend upon the binding energies of these nuclei. As the electron capture on protons has different neutrino emission characteristics than the capture on nuclei, the emitted spectra will be different for different admixtures of these components. The nuclear equation of state (EOS) controls the heights and the centroids of the neutrino spectrum such as the example shown in Fig. 1. This example was computed using the EOS, in particular the expressions for nucleonic chemical potentials as given by Fuller (1982).

Whether most of the electron captures occur on free protons or on heavy nuclei, during the collapse, depends also on the entropy of the core. At relatively low entropies (e.g. $S/k_B \approx 1$) captures on heavy nuclei dominate the total rate. Such entropies of the core do occur for stars of main sequence mass 10–25 $M_\odot$. As the entropy connected with nuclear excitations and the entropy of the free nucleons form a significant part of the total entropy of the stellar core, this is another reason for evaluating the nuclear properties of the stellar core with accuracy. The relevant temperature range of the stellar core is approximately 0.2 to 1.5 MeV at such low entropies for a density range of 10^9 – 10^{12} g/cm^3.

Investigations on the equation of state of supernova matter have by now spanned several decades (Bethe et al. 1979, hereafter BBAL; Lamb et al. 1978, hereafter LLPR78; Lattimer et al. 1985, hereafter LPRL85; Lamb et al. 1983, hereafter LLPR83). At the same time, ever since the discovery of neutron stars as pulsars more than thirty years ago, work on the equation of state of "cold, catalyzed" matter, i.e. matter at zero temperature and under thermodynamic equilibrium, has been pursued by a number of scientists (see Pethick & Ravenhall 1995 and references therein). The equation of state of hot supernova matter has been in many ways an extension of the early work done on the EOS of neutron star matter at zero temperature (Baym et al. 1971a (BPS); Baym et al. 1971b (BBP)). Since these investigations were based on the liquid drop mass formulae of Myers & Swiatecki (1966), the calculations of the equations of state for supernova have also followed largely this semi-empirical approach. More recent attempts of the EOS of supernova matter by Swesty et al. (1994) are based on the finite temperature, compressible liquid droplet model which attempts to take into account the nucleon-nucleon interaction in analogy to the density dependent Skyrme type energy functionals. On the other hand, there are microscopic investigations based on the Hartree-Fock or on the Hartree-Fock-Bogoliubov scheme with effective nucleon-nucleon interactions, such as that of Negele & Vautherin (1973) above the neutron drip point or that of Haensel et al. (1989) below the neutron drip point.

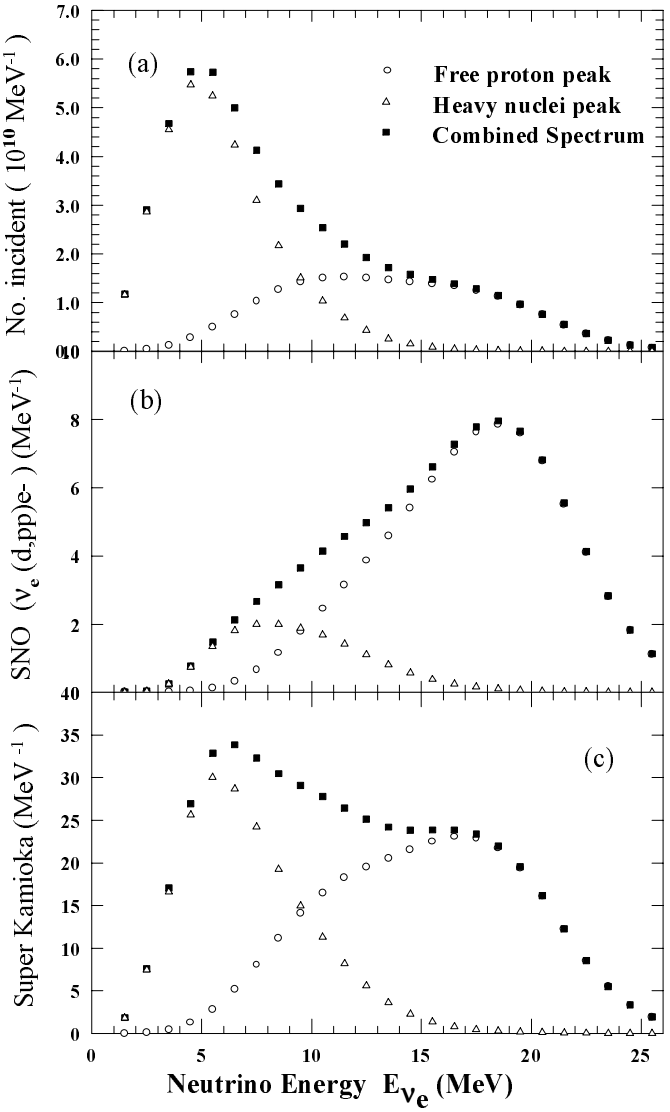

Fig. 1. **a** Cumulative neutrino flux up to $\rho_{10} = 24.16$ g/cm^3, computed with Fuller/BBAL EOS for M = 25 M$_\odot$, D = 1 kpc and $|M_{GT}|^2$ = 2.5 and later 0.1. **b** The spectrum in (**a**) is folded with the detection cross-section for c.c. reaction $\nu_e(d, pp)e^-$ in SNO. **c** The spectrum in (**a**) is folded with the detection cross-section for $\nu_e - e^-$ scattering in Super Kamioka. The projected lower limit E_ν is $\geq$ 5 MeV for the S-K and SNO detectors.

However, as far as pre-supernova conditions are concerned, the liquid-drop (or droplet) based versions of the EOS cannot be applied so easily because in this temperature range (0.2 to 1.5 MeV) shell and pairing effects dominate the nuclear structure. It is only at temperatures beyond $\sim$ 1.0to 1.5 MeV, that nuclei can be dealt within the liquid drop approximation. Thus an equation of state which is used to calculate nuclear properties in the pre-supernova stage should take into account "microscopic" shell and pairing effects. At higher temperatures and densities, well after neutrino trapping at 10^{12} g/cm^3 they should smoothly go over into the high-temperature high-density EOS based on the liquid drop model of nuclear matter. Furthermore

the computation of the EOS by theoretical methods needs to be supplemented by experimental data and their trends.

In this context, we note the work of El Eid & Hillebrandt (1980) (hereafter EH) which computed the equation of state of supernova matter and made use of the so called droplet model (DM) and its extension. The DM model was an early attempt which went beyond the conventional liquid drop model (LDM) also due to Myers & Swiatecki (1966) with the inclusion of a shell correction term due to von Groote et al. (1976). The LDM was used for the EOS computations of much of the subsequent works mentioned below. The Droplet Model is an analytical extrapolation of the Thomas Fermi model. Von Groote et al. also gave a new fit to the DM parameters to all nuclear masses known at that time. In this paper, we present a microscopic calculation based on a suitably generalized Relativistic Mean Field theory adapted to the stellar collapse problem (we refer also to Sutaria (1997), Ray et al. (1999) and Sutaria et al. (1997)). This automatically accounts for the nucleon-nucleon interactions and for shell and pairing effects, and as we show later reproduces the currently known nuclear masses with substantial accuracy. A microscopic approach like this is expected to be more reliable for nuclei relevant in the astrophysical context, which are often very neutron rich and are thus far from the valley of β-stability.

In Sect. 2 we summarise the existing equations of state based on the liquid drop approach; this helps to establish the notation and to compare with previous approaches. In Sect. 3 we describe the Relativistic Mean Field theory calculations as adapted to the supernova context. In this section we also present the results of these investigations. In Sect. 4 we compare our results with those of liquid drop based models and compare with the earlier work of Cooperstein & Baron (1990) and references therein. In Sect. 5 we describe the generalization to finite temperature and discuss the modification of our results due to low but finite temperature effects. In the concluding Sect. 6 we make a comparison with the results of EH and ours at the initial stage of stellar collapse and summarize our conclusions.

2. Suitable equations of state for each stage of the collapse

The initial efforts to compute the EOS, and indeed most of the literature available so far on the EOS of supernovae concentrate mainly on matter at densities beyond 10^{13} g/cm^3. Most of them are based on the liquid drop model of the nucleus, as the initial work of BBAL, LLPR and their co-workers. Later finite temperature extensions of the existing EOS as for instance the work of Baron et al. (1985) (hereafter BCK) and Cooperstein (1985) took into account the nuclear compressibility. The most sophisticated attempts in developing an equation of state at higher temperatures and higher densities, close to nuclear saturation densities, have been finite temperature Hartree Fock calculations, as those of Bonche & Vautherin (1981). These Hartree-Fock approaches rely on the spherical approximation and on phenomenological models for the nuclear potentials, usually of Skyrme type, which are fitted carefully to properties of finite nuclei.

As discussed in Sect. 1, the composition of stellar matter at densities between 10^7 and 10^{12} g/cm^3 and at temperatures between 0.2 and 1 MeV can be approximated by a 'soup' of nuclei including drip neutrons, protons, alpha-particles and an ensemble of heavy nuclei. The nuclear abundances in this pre-supernova stage with a density $\rho \approx 10^7$ g/cm^3 peak in two regions of the isotope table, one around the silicon group and the other around the iron group. The nuclear species in each of these groups remain in quasi-equilibrium among themselves but the groups of nuclei are not in quasi-equilibrium with each other at the lower densities (Hix & Thielemann 1996). The fraction of drip nucleons remains low during the collapse until nuclei merge into a uniform nucleon sea, possibly through a bubble phase. This is because the entropy per nucleon of the system remains close to 1 (in units of k_B) implying a high degree of order in the system (BBAL).

In the macroscopic incompressible liquid drop approach to the cold EOS above the neutron drip (BBAL 1979; BBP 1971), the ensemble of heavy nuclei and drip nucleons is considered on a lattice of number density n_N consisting of a single heavy nucleus with mass and charge numbers (A,Z) having a nuclear volume V_N immersed in a sea of drip neutrons of density n_n and electrons of density n_e. For such a system, the effective free energy density E_{tot} at zero temperatures (the internal energy density of the system), is given by BBP:

$$E_{tot}(A, Z, n_N, V_N, n_n) = n_N(W_N + W_L) + (1 - V_N n_N)E_n(n_n) + E_e(n_e). \quad (1)$$

W_L is the Coulomb lattice energy of the system, $(1 - V_N n_N)$ is the fraction of the total volume occupied by the neutron gas, E_n is the energy density of the non-relativistic free nucleon gas consisting primarily of drip neutrons and $E_e(n_e)$ is the energy density of the relativistic electrons.

The lattice energy of the system, assuming a bcc lattice structure, is expressed as $W_L = -1.82Z^2e^2/a$, where $a = (2/n_N)^{1/3}$ is the lattice constant. The quantity W_N is the nuclear matter energy of a nucleus in equilibrium with the free neutron gas, and is given by BBP:

$$W_N = [(1-x)m_n + xm_p]c^2A + [W + W_{thick} + W_{exch}]A + W_{surf}A^{\frac{2}{3}} + W_{c,0}Z^2A^{-\frac{1}{3}} \quad (2)$$

where x is the proton fraction of the heavy nucleus, m_n and m_p are neutron and proton masses, W is the energy of bulk nuclear matter per nucleon, W_{surf} is the coefficient of the surface energy term and $W_{c,0}$ is the nuclear Coulomb energy, which is taken to be the Coulomb energy of a uniformly charged sphere with charge Z. There are two corrections to the total Coulomb energy; a term due to the finite surface thickness which is denoted by $W_{thick}A$, and another due to the proton exchange term $W_{exch}A$, but both these are generally negligible (BBP). The total nuclear energy W_N, including the corrections due to lattice energy term (because the system consists of a lattice of positively charged nuclei sitting in a sea of electrons) and the 2nd order corrections to this lattice energy (due to the non-zero Coulomb radius) is given in terms of of the proton fraction x, the

density in the nuclear interior ρ_N, the nuclear volume V_N and the packing fraction i.e. the fraction of total volume occupied by nuclei ($u = \rho/\rho_N$), as (Bethe et al. 1983, hereafter BBCW):

$$W_N(x,\rho_N,V_N,u) = W_{bulk} + 290x^2(1-x)^2A^{\frac{2}{3}} + \beta x^2\rho_N^2V_N^{\frac{5}{3}}(1-\frac{3}{2}u^{\frac{1}{3}}+\frac{1}{2}u), \quad (3)$$

where the factor $\beta \simeq 3/5$, and W_{bulk} is the energy of infinite nuclear matter without surface or Coulomb, but with asymmetry effects, given in BBCW:

$$W_{bulk} = [-16 + 29.3(1-2x)^2], \quad (4)$$

The above expression for W_{bulk} is based on the simple *incompressible* liquid drop mass formula. The first term is the volume energy of the nucleus per nucleon. The second term represents the nuclear volume asymmetry energy and the coefficient of the volume asymmetry energy S_v. Here we use the value $S_v = 29.3$ obtained in the literature from fits to the experimentally known nuclear masses (Swesty et al. 1994).

The mass number A of the most dominant nuclear species is determined by a minimum of the free energy with respect to A at constant x, n_NA, n_NV_N, n_n. This leads to the conditions that the most stable nuclear system (for a given e$^-$-fraction $Y_e = x$, drip neutron density n_n, packing fraction u and heavy nuclei density $\rho_N \simeq n_NA$) is that for which the surface energy is twice the Coulomb energy: $W_{surf} = 2W_{coul}A$.

The chemical potential of the neutrons μ_n is defined as the change in the nuclear energy when a single neutron is added to the nucleus, keeping the number of protons constant. Therefore μ_n can be obtained from Eq. (3) by

$$\mu_n = \frac{1}{V_N}\left(\frac{\partial W_N}{\partial \rho_N}\right)_{x,V_N,u} - \frac{x}{A}\left(\frac{\partial W_N}{\partial x}\right)_{\rho_N,V_N,u}, \quad (5)$$

and similarly, the difference of neutron and proton chemical potentials is obtained by:

$$\hat{\mu} = \mu_n - \mu_p = -\frac{1}{A}\left(\frac{\partial W_N}{\partial x}\right)_{\rho_N,V_N,u} \quad (6)$$

Using Eqs. (5) and (6) along with Eq. (3) and the condition that the surface energy is twice the Coulomb energy for the "mean nucleus", one can obtain relations for μ_n and $\hat{\mu}$. Fuller (1982), quoting a private communication from Lattimer (1980) gives an expression for μ_n as:-

$$\mu_n = -16 + 125(0.5-x) - 125(0.5-x)^2 - 290\frac{x^2(1-x)^2(3-7x)}{A^{1/3}2(1-x)} \quad (7)$$

and for $\hat{\mu}$ as (BBAL):-

$$\hat{\mu} = 250(0.5-x) - \frac{290}{A^{1/3}}x^2(1-2x)^2\left(\frac{1}{x}+\frac{2}{x}\frac{1-2x}{1-x}\right) \quad (8)$$

Note however the comments pertaining to these, discussed in the next section. This model described in Eqs. (1 - 8) (cited as BBAL/BBP-EOS later on) is based on an incompressible liquid drop. It uses the surface energy term of Ravenhall et al. (1972) and it assumes that the actual nuclear density can be approximated by the nuclear density at saturation. The relations for μ_n are taken from Fuller (1982) and are meant for near-symmetric nuclear matter for which $x \simeq 0.5$. The correction terms in μ_n are discussed in the next section. In Fig. 2 we display the LDM expression of Eq. 7 for the chemical potential of the neutrons in the chain of Mn-isotopes along with the values obtained form relativistic mean field calculations $\mu_n|_{RMF}$ which will be discussed later. Similar diagrams for the elements Fe, Co, Ni, Cu, Zn, Ga, and Ge can be found in Sutaria (1997). For the curve labeled BCK in Fig. 2, modifications were made to take into account the difference between the actual nuclear density and the saturation density in the compressible EOS developed by Baron et al. (1985) (BCK) and Cooperstein (1985) (cited as BCK-EOS lateron).

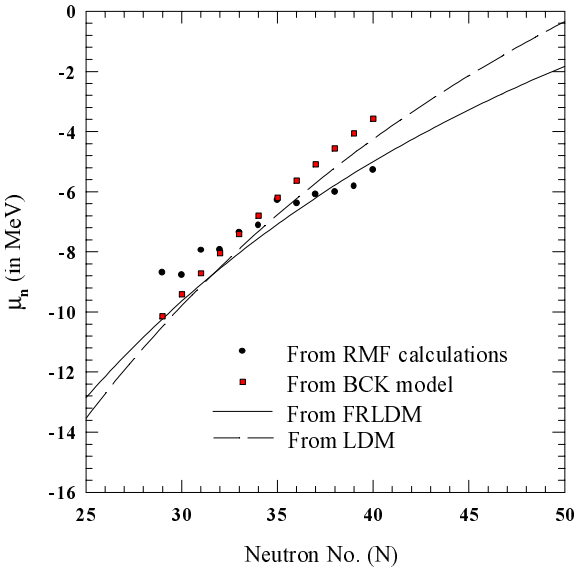

Fig. 2. The chemical potential of our RMF-calculations with the parameter set NL-SH $\mu_n|_{RMF}$ is compared with that of the BCK-model $\mu_n|_{BCK}$ and with the functional forms of the liquid drop model (LDM) given in Eq. (7) and the finite range liquid drop model (FRLDM) $\mu_n|_{FRLDM}$ discussed in Sect. 4.2 for Mn isotopes

The BCK-EOS differs from the BBAL/BBP-EOS in three points: (a) a term is incorporated in the expression for W_N/A which takes into account the nuclear compressibility, (b) the actual nuclear density ρ_0 may differ from the saturation nuclear density of infinite nuclear matter ρ_s, (c) ρ_s is allowed to depend on the proton fraction x, where the functional form of this dependence ($\phi(x) = \rho_s(x)/0.16\ \mathrm{fm}^{-3} = 1$–$3(0.5-\mathrm{x})^2$) was obtained by fits to the density dependent HF calculations with the force SKM of Bonche & Vautherin (1981). In the compressible model, the expression for W_N has the form:

$$W_N = -16 + 29.3\,(1-2x)^2 + \frac{1}{18}K(1-\theta)^2 + 75.4\,x^2(1-x)^{\frac{4}{3}}\phi^{-\frac{1}{3}}\theta^{-\frac{1}{3}}\left(1-\frac{3}{2}u^{\frac{1}{3}}+\frac{1}{2}u\right)^{\frac{1}{3}} \quad (9)$$

Where K is the coefficient of nuclear compressibility, $\theta = \rho_0/\rho_s$ is the ratio of the actual nuclear density ρ_0 to the saturation nuclear density ρ_s, and u is the packing fraction of the nuclei, such that $u = \rho/\rho_0$. The term dependent on the compressibility was added in order to obtain an accurate description of the phase transition into the bubble region without producing any discontinuities in the pressure or the temperature variables in the numerical calculations simulating the core collapse. The low entropy liquid drop-based equations of state (hereby the LDM-EOS) all apply to warm dense matter. The approaches vary: BBAL use the phenomenological approach, which included many basic features of the microscopic calculations of LPRL. BCK use the "top down" route, where the relevant nuclear parameters like bulk incompressibility, saturation density including its dependence on Y_e, on the nucleon effective mass, or the bulk asymmetry energy coefficients, etc. were taken as input quantities for the calculation of thermodynamic variables, rather than as output for a specific set of nuclear force parameters, as in the microscopic calculation. The BCK series of EOS were constructed for numerical applications in supernova hydrodynamics and therefore with physical and numerical simplicity as important considerations. The composition of warm dense matter is determined under the conditions of mass and charge conservation, by the pressure balance at the surface of a heavy nucleus surrounded by light nuclei like α-particles and by a "vapour" of free protons and neutrons, and under the assumption that the strong and electro-magnetic reactions have reached nuclear statistical equilibrium (NSE) (Cooperstein & Baron 1990).

An explicit dependence on temperature was introduced in the BCK-EOS free energy (F) term by using the expression:

$$F = W_N - \frac{a}{A}\frac{m^*}{m}T^2 \tag{10}$$

where m^*/m is the effective mass of the nucleons in the nucleus and a is level density parameter in the Fermi-gas model of the nuclei.

3. The relativistic mean field (RMF) approach

The Hartree-Fock (HF) or Hartree-Fock-Bogoliubov (HFB) methods of calculating nuclear properties depend on the knowledge of a suitable nuclear potential. Usually Skyrme or Skyrme-type forces are used for this purpose. In recent years the microscopic description of ground state properties of finite nuclei has been attempted by a relativistic field theory for the nuclear many-body problem. Reviews of this work have been given by Serot & Walecka (1986) and Gambhir et al. (1990).

Relativistic Mean Field Theory starts from an effective Lagrangian containing the nucleonic and mesonic degrees of freedom. It is a relativistic analogue of the concepts of density dependent Hartree-Fock calculations with Skyrme forces. Because of its proper treatment of the spin-orbit splitting this model is expected to be more reliable than the non-relativistic models in predicting yet unknown properties of nuclei far from stability which are important in astrophysical situations. Also in some respects this method is simpler than the Skyrme type calculations, since the RMF method involves only local quantities such as local densities and fields. The binding energies and nuclear charge radii calculated by these methods agree well with the experimental values (see e.g. Table 1). The density distributions of doubly magic spherical nuclei also agree well with electron scattering data. In addition, apart from the ground state properties of spherical nuclei, RMF reproduces the right ordering of the single particle spectra in adjacent odd mass nuclei, without any additional parameters. It also describes in a quantitative way nuclear deformations and superdeformations.

The microscopic RMF approach is used here to calculate nuclear properties at zero temperature, both for isolated nuclei, an approximation which holds well at the end of the Si-burning stage as well as for the case with higher density but still zero temperature where the nuclei can be assumed to be distributed in a lattice, and where modifications due to Lattice Coulomb energy have to be taken into account.

Within relativistic mean field theory (Sheikh et al. 1993) the nucleus is described by an ensemble of nucleons caracteristic by Dirac spinors and moving independently in self-consistently determined meson- and electro-magnetic fields. The Lagrangian, describing this system is given by

$$\mathcal{L} = \mathcal{L}_B + \mathcal{L}_M + \mathcal{L}_{BM}, \tag{11}$$

Table 1. The nuclear charge radii for Ni isotopes. The table gives the experimental values and those computed in this work from RMF calculations with the parameter sets NL1 and NL-SH.

Neutron number	Experimental Nadjakov et al. (1994)	RMF (NL1)	RMF (NL-SH)
30	3.7827 ± 0.0036	3.804	3.791
32	3.8177 ± 0.0047	3.797	3.794
33	3.8283 ± 0.0030	3.805	3.802
34	3.8475 ± 0.0050	3.812	3.809
36	3.8678 ± 0.0051	3.830	3.826

Table 2. The parameter set for macroscopic FRLDM model

Quantity	Brief definition	Value (Unit)
a_v	Volume energy constant.	16.00126 MeV
κ_v	Volume asymmetry constant.	1.9224 MeV
a_s	Surface energy constant.	21.18466 MeV
κ_s	Surface asymmetry constant.	2.345 MeV
a_0	A^0 constant.	2.615 MeV
c_a	Charge asymmetry constant.	0.10289 MeV
r_0	Nuclear-radius constant.	1.16 fm
r_p	Proton r.m.s. radius.	0.80 fm
a	Range of Yukawa-plus-exponential potential.	0.68 fm
a_{den}	Range of Yukawa function for generating charge distribution.	0.70 fm
e^2	square of the e^--charge	1.4399764 MeV fm

with

$$\mathcal{L}_B = \overline{\psi}_i(i\gamma^\mu\partial_\mu - m_N)\psi_i, \quad (12)$$

$$\mathcal{L}_M = \frac{1}{2}\partial^\mu\sigma\partial_\mu\sigma - U(\sigma) - \frac{1}{4}\Omega^{\mu\nu}\Omega_{\mu\nu} + \frac{1}{2}m_\omega^2\omega^\mu\omega_\mu - \frac{1}{2}\tilde{R}^{\mu\nu}\tilde{R}_{\mu\nu} + \frac{1}{2}m_\rho^2\tilde{\rho}^\mu\tilde{\rho}_\mu - \frac{1}{2}F^{\mu\nu}F_{\mu\nu}, \quad (13)$$

$$\mathcal{L}_{BM} = -g_\sigma\overline{\psi}_i\psi_i\sigma - g_\omega\overline{\psi}_i\gamma^\mu\psi_i\omega_\mu - g_\rho\overline{\psi}_i\gamma^\mu\tilde{\tau}\psi_i\tilde{\rho}_\mu - e\overline{\psi}_i\gamma^\mu\frac{1-\tau_3}{2}\psi_iA_\mu. \quad (14)$$

m_N is the nucleon mass, m_σ, m_ω, and m_ρ are the masses of the σ-, ω- and ρ-mesons, g_σ g_ω and g_ρ are the corresponding meson-nucleon coupling constants. Tilde indicate the isospin degree of freedom and $\Omega^{\mu\nu}$, $\tilde{R}_{\mu\nu}$, $F_{\mu\nu}$ are the field tensors. $U(\sigma)$ is the non-linear potential for the σ mesons. It takes into account the density dependence in a phenomenological way and it has the form (Boguta & Bodmer 1977):

$$U(\sigma) = \frac{1}{2}m_\sigma^2\sigma^2 + \frac{1}{3}g_2\sigma^3 + \frac{1}{4}g_3\sigma^4 \quad (15)$$

For the three mass parameters m_N, m_ω and m_ρ entering the Lagrangian we use the experimentally known values. In general, the other parameters are obtained by fitting ground-state binding energies and charge radii of a few spherical nuclei. Several sets of such parameters are given in the literature. The parameter set NL1 (Reinhard et al. 1986) has turned out to be very successful in the valley of β-stability. Here we use the parameter set NL-SH, which was obtained by fitting the binding energy, the charge-radii and also the neutron-skin radii of a few spherical nuclei (Sharma et al. 1993). In Table 1 we show that both the NL1 and the NL-SH parameter sets reproduce well the experimentally known nuclear charge-radii (Nadjakov et al. 1994) of Ni isotopes. We also compare (see Table 7) with results obtained from the more recently determined parameter set NL3 (Lalazissis et al. 1997), which is often used in the literature for the study of exotic nuclei.

While the set NL-SH reproduces well nuclear binding energies, we find that the incompressibility coefficient K_0 of bulk nuclear matter as predicted by the set NL-SH is much larger than the value adopted earlier, where a value of $K_0 = 180$ MeV has been used e.g. in BCK.

A comparison of the neutron chemical potentials μ_n with the results of the compressible liquid drop model suggests that the RMF results are not very sensitive to the value of the adopted compressibility coefficient. (see Sect. 4).

However, it is to be noted that the results presented in this work are meant to apply to physical conditions prevalent in the collapsing core up to $\rho = 10^{12}$ g/cm^3, i.e. well below the density at which the core reaches maximum compression and rebounds. Since the nuclear composition of the core at this stage can still be treated as consisting of individual nuclei plus Coulomb lattice corrections, one may use a relatively high value of bulk compressibility as in NL-SH without worrying too much about the effects that it may have on the strength of the shock generated by the re-bouncing core.

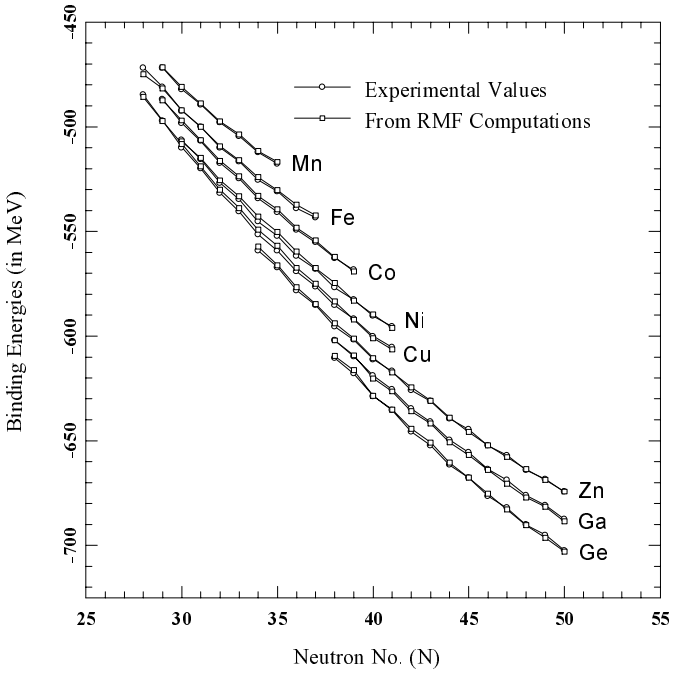

Fig. 3. Experimental vs. calculated values of binding energies using the parameter set NL-SH.. The calculations were carried out with the the pairing gap parameters listed in the Tables 3, 4, 5 and 6.

Since mean-field calculations take into account only the long-range part of the nucleon-nucleon interaction the short-range pairing correlations have to be incorporated in addition. In the present work, the simplistic monopole pairing interaction is used and the resulting equations are solved in the BCS approximation. Because the value of the coupling constant in the pairing interaction is not known precisely, pair-gaps obtained from odd-even mass differences are generally used as a measure of the pairing strength. Initially, the calculations were started off using pair-gaps obtained by the 4-point method of Bohr & Mottelson (1969) from the experimental values of the binding energies, wherever known. However, the experimental binding energies are not known for most of the nuclei of interest and we have adopted the pair-gaps suggested by Möller et al. (1995) using isospin asymmetry arguments. For the cases where the experimental binding energies are known, these and the theoretically computed binding energies are displayed in Fig. 3.

In cases where multiple energy solutions were obtained, the solution corresponding to the lowest energy was taken as our preferred solution. It is found that deformations of the lowest energy solution predicted by the RMF calculations are similar to those predicted by the Finite Range Droplet Model (FRDM) in Möller et al. (1995), which leads in this case practically to the same results as the Finite Range Liquid Drop Model (FRLDM).

The values of the pairing gaps Δ_n and Δ_p used in the entire series of calculations have been recorded in Tables 3, 4, 5 and 6 for a series of isotopes ranging from $^{54}\mathrm{Mn}_{25}$ to $^{81}\mathrm{Ge}_{32}$. We also show in these tables the calculated values of the quadrupole deformation beta β, the binding energies BE_{RMF} and the chem-

Table 3. Results of RMF calculations for various isotopes of Mn and Fe, giving the values of μ_n, μ_p and the deformation parameter β. Also tabulated are the values of the fixed neutron and proton pairing-gaps (Δ_n and Δ_p) used in these calculations. The last two columns display the experimental and calculated values of the binding energies ($BE_{\rm Exp.}$ and $BE_{\rm RMF}$ respectively)

Isotope	Δ_n	Δ_p	μ_n	μ_p	β	$BE_{\rm Exp.}$	$BE_{\rm RMF}$
$^{54}Mn_{25}$	1.00	1.50	-8.6790	-8.6260	0.1265	-471.84940	-471.64801
$^{55}Mn_{25}$	1.00	1.50	-8.7800	-9.2290	0.2082	-482.07599	-480.91101
$^{56}Mn_{25}$	1.20	1.50	-7.9420	-9.9240	0.2187	-489.34659	-488.92999
$^{57}Mn_{25}$	2.00	1.50	-7.9260	-10.5230	0.2091	-497.99701	-497.51801
$^{58}Mn_{25}$	1.20	1.50	-7.3470	-11.4300	0.2213	-504.41000	-503.65399
$^{59}Mn_{25}$	2.00	1.25	-7.1270	-11.9500	0.2130	-512.12903	-511.54700
$^{60}Mn_{25}$	1.20	1.25	-6.2840	-12.8120	0.2110	-517.62000	-516.78497
$^{61}Mn_{25}$	2.00	1.25	-6.3820	-13.1600	0.1896	–	-524.057
$^{62}Mn_{25}$	1.25	1.25	-6.0970	-13.7840	0.1354	–	-528.286
$^{63}Mn_{25}$	1.50	1.00	-6.0110	-14.3490	0.1097	–	-534.347
$^{64}Mn_{25}$	1.00	0.50	-5.8150	-15.0530	0.0830	–	-539.142
$^{65}Mn_{25}$	0.75	0.50	-5.2780	-15.5570	0.0458	–	-544.673
$^{54}Fe_{26}$	2.50	1.50	-12.0530	-7.1700	0.0003	-471.76392	-470.85400
$^{55}Fe_{26}$	1.50	2.50	-10.5820	-7.8950	0.0000	-481.06192	-481.15302
$^{56}Fe_{26}$	2.50	2.50	-9.5510	-8.2400	0.0000	-492.25992	-492.17700
$^{57}Fe_{26}$	2.00	2.50	-8.9800	-8.7980	0.1531	-499.90610	-500.02802
$^{58}Fe_{26}$	2.50	2.50	-8.7690	-9.3750	0.1514	-509.95081	-509.32599
$^{59}Fe_{26}$	2.00	2.00	-8.1790	-10.0260	0.1915	-516.53180	-515.96600
$^{60}Fe_{26}$	2.25	2.00	-7.8740	-10.6300	0.1839	-525.34802	-524.05402
$^{61}Fe_{26}$	1.75	2.00	-7.2590	-11.3220	0.1853	-530.93201	-530.29102
$^{62}Fe_{26}$	2.00	2.00	-7.1360	-11.9780	0.1421	-538.97998	-537.29602
$^{63}Fe_{26}$	1.75	1.75	-7.0720	-13.0450	-0.0938	-543.34998	-542.30103

ical potentials μ_n and μ_p. The binding energies are compared with the experimental values $BE_{Exp.}$ The data for the Ni isotopes is especially useful because these isotopes are spherical and in later sections we will compare the RMF calculations with macroscopic models as the macroscopic liquid drop model (BBAL, BBCW), which do not take into account effects due to deformation.

In Table 7 we present for the chain of Ni-isotopes calculations with the parameter set NL3 Lalazissis (1997). For most of the elements in this chain the binding energies obtained with the new parameter set NL3 are somewhat better, the set NL-SH however seems to be superior for very large neutron excess. Comparing with table 4 we find for the chemical potentials relatively small differences of around 100–200 keV between the two parameter sets. We therefore do not expect dramatic changes in using the parameter set NL3 as compared to NL-SH, which is applied in all the other investigations in this work.

How was this range of isotopes chosen? The significant difference of nuclei in the collapsing core from those in the laboratory is that the former are more neutron-rich. The typical electron fraction $\rm Y_e$ ranges from 0.42 to 0.38 in the early stages of the collapse rather than from 0.46 to 0.5 as is the case with the more symmetric laboratory nuclei. Nevertheless they are still far less neutron-rich than matter in neutron stars where the $\rm Y_e$ could be near 0.05. The nuclear statistical equilibrium gives rise to a fairly broad range of nuclei at any given instant of time, and in a given mass-zone of the collapsing core which can affect the (potentially) observable neutrino spectrum. The range of nuclei chosen here corresponds to values of the lepton fraction Y_l, which for this pre-trapping range of temperatures and densities, equals the electron fraction Y_e, ranging from 0.42 to 0.38. They are all mid-$f-p$ shell nuclei which have been shown (Hix & Thielemann 1996) to dominate the core nuclear configuration for this stage of the stellar evolution.

4. Comparison of chemical potentials

If a detailed simulation of the stellar collapse is carried out, where electron-capture and beta decay rates of individual nuclei have to be taken into account in a network calculation, the EOS based on macroscopic spherical liquid-drop models cannot be expected to reproduce accurately (i.e. with a deviation of approximately 1 MeV) the nuclear chemical potentials (μ_n, μ_p and $\hat{\mu}$) and binding energies (the W_N values) in the low-density region. In the following sections we investigate the amount of deviation that can be expected due to shell effects and pairing correlations on nuclear properties under stellar conditions. We also discuss the possible improvements which can be made on W_N using more advanced versions like the macroscopic-microscopic mass formulae, e.g. the Finite Range Liquid Droplet Model (FRLDM) of Möller et al. (1995), which account for deformation effects.

The RMF computations presented in Sect. 3 are compared here with values of μ_n and $\hat{\mu}$ calculated from the models discussed in the previous sections, extended to the case of isolated nuclei, i.e. ignoring the lattice corrections. Comparison is also made between RMF calculations and the finite temperature

Table 4. Results of RMF calculations for various isotopes of Co and Ni, giving the values of μ_n, μ_p and the deformation parameter β. Also tabulated are the values of the fixed neutron and proton pairing-gaps (Δ_n and Δ_p) used in these calculations. The last two columns show the experimental and calculated values of binding energies.

Isotope	Δ_n	Δ_p	μ_n	μ_p	β	$BE_{\rm Exp.}$	$BE_{\rm RMF}$
$^{56}Co_{27}$	1.00	1.50	-9.2070	-7.1380	0.0003	-487.96399	-486.91150
$^{57}Co_{27}$	1.02	1.50	-9.6860	-7.2640	0.1408	-497.01001	-498.28741
$^{58}Co_{27}$	1.17	1.50	-9.2300	-7.7340	0.1675	-506.35599	-506.86050
$^{59}Co_{27}$	2.00	1.50	-9.1760	-8.4530	0.1430	-516.29102	-517.31409
$^{60}Co_{27}$	1.20	1.25	-8.6380	-8.8190	0.1820	-523.69702	-524.80615
$^{61}Co_{27}$	2.00	1.25	-8.4150	-9.6480	0.1520	-532.99597	-534..12738
$^{62}Co_{27}$	1.15	1.25	-7.6400	-10.1580	0.1640	-539.52698	-540.72498
$^{63}Co_{27}$	2.00	1.25	-7.9050	-11.4190	0.0915	-548.28497	-549.21198
$^{64}Co_{27}$	1.20	1.25	-7.8090	-12.4110	0.0455	-554.36798	-555.23602
$^{65}Co_{27}$	1.50	1.00	-7.4920	-13.2190	0.0011	-562.22900	-562.67999
$^{58}Ni_{28}$	2.50	2.50	-10.8710	-5.7110	0.0000	-507.02899	-506.45901
$^{59}Ni_{28}$	2.00	2.00	-9.9250	-6.3600	0.0000	-514.91101	-515.45892
$^{60}Ni_{28}$	2.50	2.00	-9.8810	-6.9550	0.0000	-525.61603	-526.84735
$^{61}Ni_{28}$	2.00	2.00	-9.3950	-7.6600	0.0000	-533.20502	-534.66760
$^{62}Ni_{28}$	2.25	1.75	-9.2210	-8.2490	0.0000	-542.88800	-545.26501
$^{63}Ni_{28}$	1.75	1.50	-8.9080	-8.9340	0.0000	-550.31299	-552.10352
$^{64}Ni_{28}$	2.00	1.50	-8.6650	-9.4930	0.0000	-559.63000	-561.76013
$^{65}Ni_{28}$	1.75	1.50	-8.3620	-10.1220	0.0000	-567.52698	-567.85834
$^{66}Ni_{28}$	1.00	1.00	-8.0750	-10.7160	0.0000	-574.58398	-576.83301
$^{67}Ni_{28}$	1.50	1.00	-7.5840	-11.2130	0.0000	-583.01501	-582.61902
$^{68}Ni_{28}$	0.75	1.00	-6.9360	-11.7330	0.0000	-589.70001	-590.42999

Table 5. Results of RMF calculations for various isotopes of Cu and Zn, giving the values of μ_n, μ_p and the deformation parameter β. Also tabulated are the values of the fixed neutron and proton pairing-gaps (Δ_n and Δ_p) used in these calculations, as well as the experimental and calculated values of the binding energies.

Isotope	Δ_n	Δ_p	μ_n	μ_p	β	$BE_{\rm Exp.}$	$BE_{\rm RMF}$
$^{57}Cu_{29}$	1.00	1.50	-14.0190	-1.3950	-0.0009	-484.76001	-485.70700
$^{58}Cu_{29}$	2.00	1.75	-11.0700	-2.5080	0.0037	-497.11401	-497.35001
$^{59}Cu_{29}$	2.00	1.75	-11.2610	-4.0470	0.1461	-509.87601	-508.19299
$^{60}Cu_{29}$	2.00	1.75	-10.6050	-4.9190	0.1650	-519.93811	-518.96899
$^{61}Cu_{29}$	2.25	1.75	-10.5020	-5.3060	0.1394	-531.64679	-530.08899
$^{62}Cu_{29}$	1.75	1.75	-9.8260	-6.3300	0.1750	-540.53400	-538.87299
$^{63}Cu_{29}$	2.50	1.50	-9.6850	-6.4610	0.1374	-551.38715	-549.16901
$^{64}Cu_{29}$	2.00	1.50	-9.0460	-7.2040	0.1424	-559.30316	-556.85797
$^{65}Cu_{29}$	2.25	1.50	-9.1590	-7.3710	-0.1001	-569.21216	-567.38501
$^{66}Cu_{29}$	1.50	1.50	-8.8200	-8.0180	-0.0922	-576.27814	-574.91803
$^{67}Cu_{29}$	2.25	1.25	-8.5780	-7.9580	-0.0083	-585.39697	-583.46503
$^{64}Zn_{30}$	2.50	2.50	-10.6040	-5.8830	0.1700	-559.09912	-557.58899
$^{65}Zn_{30}$	2.00	2.50	-9.8550	-6.7130	-0.1663	-567.07898	-566.32001
$^{66}Zn_{30}$	2.50	2.50	-9.7730	-7.0710	-0.1314	-578.13885	-576.87000
$^{67}Zn_{30}$	2.00	2.50	-9.4760	-7.5290	-0.1161	-585.19086	-584.99200
$^{68}Zn_{30}$	2.25	2.25	-9.2010	-7.8250	-0.0793	-595.38898	-593.99298
$^{69}Zn_{30}$	1.75	2.00	-8.7400	-8.2670	0.0159	-601.87122	-601.14203
$^{70}Zn_{30}$	2.25	2.00	-8.4010	-8.8290	0.0169	-611.08600	-610.53101
$^{71}Zn_{30}$	1.75	2.00	-7.8710	-9.4300	0.0090	-616.91901	-617.31897
$^{72}Zn_{30}$	2.00	1.50	-7.6870	-9.9300	0.0764	-625.80200	-624.49799
$^{73}Zn_{30}$	1.25	1.50	-7.6010	-11.0730	0.0000	-631.15002	-630.94098
$^{74}Zn_{30}$	1.50	1.50	-7.2610	-11.7630	0.0000	-639.51898	-638.95001
$^{75}Zn_{30}$	1.25	1.50	-6.9250	-12.4690	0.0000	-644.58002	-645.87000
$^{76}Zn_{30}$	1.00	1.00	-6.4360	-13.0960	0.0001	-652.41998	-652.28497
$^{77}Zn_{30}$	0.20	0.50	-5.8320	-13.7630	0.1720	-656.94000	-657.80603
$^{78}Zn_{30}$	0.50	0.50	-5.4660	-14.2850	0.1497	-664.06000	-663.66101

Table 6. Results of RMF calculations for various isotopes of Ga and Ge, giving the values of μ_n, μ_p and the deformation parameter β. Also tabulated are the values of the fixed neutron and proton pairing-gaps (Δ_n and Δ_p) used in these calculations as well as the calculated and the experimental values of the binding energies, $BE_{\rm Exp.}$ and $BE_{\rm RMF}$ respectively.

Isotope	Δ_n	Δ_p	μ_n	μ_p	β	$BE_{\rm Exp.}$	$BE_{\rm RMF}$
$^{69}Ga_{31}$	2.50	2.50	-9.7100	-7.2800	0.0897	-601.99402	-602.03601
$^{70}Ga_{31}$	1.50	2.50	-9.2860	-7.7540	0.0010	-609.64899	-609.17798
$^{71}Ga_{31}$	2.50	2.50	-9.0280	-8.3030	0.0148	-618.95618	-620.22803
$^{72}Ga_{31}$	1.50	2.50	-8.3770	-8.8990	0.0014	-625.47729	-626.45203
$^{73}Ga_{31}$	2.50	1.50	-8.4390	-9.4400	0.1686	-634.66302	-635.96198
$^{74}Ga_{31}$	1.50	1.50	-8.1890	-10.0830	0.1770	-641.08002	-641.78699
$^{75}Ga_{31}$	2.00	1.30	-7.8210	-10.5600	0.1730	-649.56598	-650.75098
$^{76}Ga_{31}$	1.00	1.10	-7.6520	-11.0730	0.1800	-655.62000	-656.83698
$^{77}Ga_{31}$	0.75	0.75	-7.1730	-11.6270	0.1790	-663.65997	-664.02197
$^{78}Ga_{31}$	0.50	0.50	-6.7420	-12.4590	0.1680	-668.88000	-670.63800
$^{79}Ga_{31}$	0.25	0.25	-6.0880	-13.3830	0.1540	-676.14001	-677.14899
$^{80}Ga_{31}$	0.20	0.20	-6.9860	-13.4700	-0.0771	-680.84003	-681.55902
$^{81}Ga_{31}$	0.20	0.20	-5.0490	-14.1430	-0.0574	-687.51001	-688.55798
$^{70}Ge_{32}$	2.50	2.50	-10.1990	-6.7730	-0.1831	-610.54401	-609.46198
$^{71}Ge_{32}$	1.00	2.50	-9.7040	-7.4030	-0.1692	-617.96600	-616.29401
$^{72}Ge_{32}$	2.50	2.50	-9.4920	-7.8830	-0.1650	-628.70801	-628.55902
$^{73}Ge_{32}$	1.00	2.50	-8.8660	-8.6950	-0.1935	-635.50000	-635.09198
$^{74}Ge_{32}$	2.00	2.00	-8.6880	-8.9680	-0.1749	-645.69202	-644.26599
$^{75}Ge_{32}$	1.00	2.00	-8.8110	-9.3880	0.1881	-652.20398	-650.90198
$^{76}Ge_{32}$	1.50	2.00	-8.4500	-9.9400	0.1721	-661.62598	-660.47302
$^{77}Ge_{32}$	1.00	1.50	-8.2590	-10.3350	0.1793	-667.69800	-667.63300
$^{78}Ge_{32}$	0.75	1.00	-7.9020	-10.8030	0.1760	-676.41998	-675.31500
$^{79}Ge_{32}$	0.50	0.25	-7.6670	-11.4350	0.1660	-682.12201	-682.85199
$^{80}Ge_{32}$	0.25	0.25	-6.7390	-12.1790	0.1530	-690.15399	-690.39801
$^{81}Ge_{32}$	0.25	0.25	-6.3290	-12.7720	0.1149	-695.07599	-696.47198

BCK-EOS, at low temperatures and densities ($\rho_{10} = 0.1$ and $T = 0.1$ MeV) using both the values of K_0 and S_v adopted by BCK in their calculations and the more recent values used by Sharma et al. (1993). These comparisons show that the binding energies as well as the neutron and proton chemical potentials have considerable differences from the values predicted by the macroscopic models of BBAL. The results from RMF calculations are in better agreement with the predictions from FRLDM calculations that are based on more recent compilations of the laboratory data on nuclei.

4.1. Comparisons with the spherical liquid-drop models

It has been stated earlier that the relations for μ_n and $\hat{\mu}$ in Eqs. (7) and (8) are applicable for nearly symmetric, incompressible nuclear matter, confined by spherical surfaces. The bulk energy term per nucleon W_{bulk} was taken to be dependent on the nuclear volume energy and on the nuclear asymmetry energy (see BBCW Eqs 2.1 to 2.10, especially 2.4) given by Eq. 4. A derivation of μ_n using this form of the bulk energy gives the following relation for the neutron chemical potential of a mean nucleus of mass no. A:-

$$\mu_n = -16 + 29.3(1-2x)^2 + 117.2\,x(1-2x) + W_{size}(x)\frac{7x-3}{3(1-x)} = \mu_n|_{vol} + \mu_n|_{size}, \quad (16)$$

where $W_{size}(x) = 75.4x^2(1-x)^{4/3}$ is the combined surface and Coulomb energy (without lattice correction, i.e. $f_\rho[u] = 1$) for the "mean nucleus" and $\rho_0(x)$ is the nuclear density. Fig. 4

Table 7. Results of RMF calculations for various isotopes of Ni using the parameter set NL3. The values of the fixed proton and neutron pair-gaps (Δ_n and Δ_p) used in these calculations are identical to the values used in calculations with parameter set NL-SH. The remaining columns give the computed values of μ_n, μ_p, and the differences between the calculated and experimental binding energies in Table 4 in MeV. Negative values mean that the calculated binding energy is larger then the experimental binding energy.

Isotope	μ_n	μ_p	$BE_{\rm NL3} - BE_{\rm Exp.}$	$BE_{\rm NL-SH} - BE_{\rm Exp.}$
$^{58}Ni_{28}$	-11.044	-5.692	0.74099	0.56998
$^{59}Ni_{28}$	-10.085	-6.282	0.60501	0.45209
$^{60}Ni_{28}$	-10.041	-6.861	0.48603	-1.23132
$^{61}Ni_{28}$	-9.527	-7.556	0.44602	-1.46258
$^{62}Ni_{28}$	-9.375	-8.101	0.31500	-2.37701
$^{63}Ni_{28}$	-9.090	-8.759	0.26599	-1.79053
$^{64}Ni_{28}$	-8.873	-9.320	-0.04600	-2.13013
$^{65}Ni_{28}$	-8.619	-9.954	-0.29802	-0.33136
$^{66}Ni_{28}$	-8.479	-10.582	-0.54602	-2.24903
$^{67}Ni_{28}$	-7.873	-11.078	-1.09099	0.39599
$^{68}Ni_{28}$	-7.133	-11.645	-1.60199	-0.42998

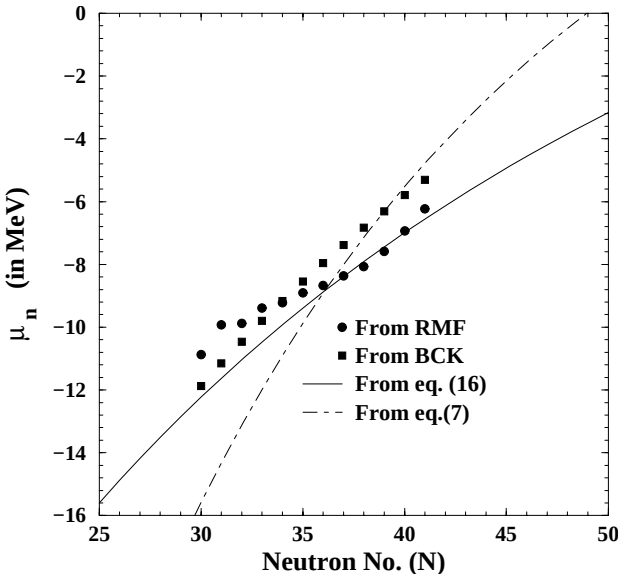

Fig. 4. Neutron chemical potentials of Ni isotopes calculated within RMF theory based on the parameter set NL-SH and within the BCK-model are compared with the functional form of μ_n in Eq. (16) (solid line) and Eq. (7) (dashed line).

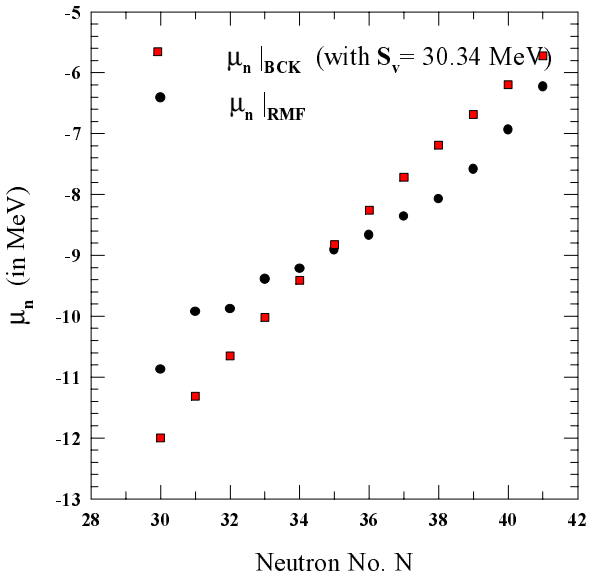

Fig. 5. The chemical potentials $\mu_n|_{RMF}$ (parameter set NL-SH) and $\mu_n|_{BCK}$ for Ni. The values $\mu_n|_{BCK}$ have been generated from the BCK-EOS using $S_v = 30.34$ MeV but with the same incompressibility $K = 180$ and $a_v = 16.0$.

displays the chemical potential obtained form Eq. (16) for Ni isotopes, alongside with their RMF and BCK-EOS counterparts. It should be noted here that because of an error in the surface terms, the μ_n from the BBAL equations do not agree well with the RMF results (in fact, they are off by up to 2 MeV).

The RMF results are also compared with the BCK-EOS in Fig. 2. For generating this set of numbers for the BCK-EOS, the density and the temperature were set at 10^9 g/cm^3 and and 0.1 MeV so that we are as close as possible to the end-stages of Si-burning, with their nuclear asymmetry energy coefficient taken as $E_S = 31.5$ MeV and the incompressibility as $K = 180$. However, the RMF calculations correspond to a incompressibility coefficient $K = 354.95$ and $S_v = 36.1$ for reasons discussed in Sect. 3. Values for the nuclear incompressibility deduced from experiments have shown a large variation, K_0 ranges from 180 to 300 MeV. Since the objective of the comparisons here is to evaluate the deviation that can be expected in the LDM-EOS (compressible and incompressible) due to exclusion of shell and pairing effects, the μ_n and $\hat{\mu}$ from BCK-EOS were recalculated using different values of S_v and K_0. It was found that the results were more sensitive to a variation in S_v than to K_0. In order to obtain a suitable value of S_v (used in BCK-EOS) which would better reproduce the RMF chemical potentials, a fit was made of the following expression of $\hat{\mu}|_{RMF}$:

$$\hat{\mu} = 4S_v(1-2x) - 290\frac{x^2(1-x)^2}{A^{1/3}}\left[\frac{1}{x} + \frac{2}{x}\frac{1-2x}{1-x}\right] \qquad (17)$$

This gives an "average" value of S_v (over the range of isotopes for Mn, Fe, Co, Ni, Cu, Zn, Ga, Ge considered in the Tables 3, 4, 5, 6) of 30.4 MeV. It is found that using the low value of $K = 180$ MeV, the "best fitted" value of S_v is 30.34 MeV. Figs. 5 and 6 compare μ_n and $\hat{\mu}$ for Ni isotopes using this parameter set in BCK-EOS with RMF results.

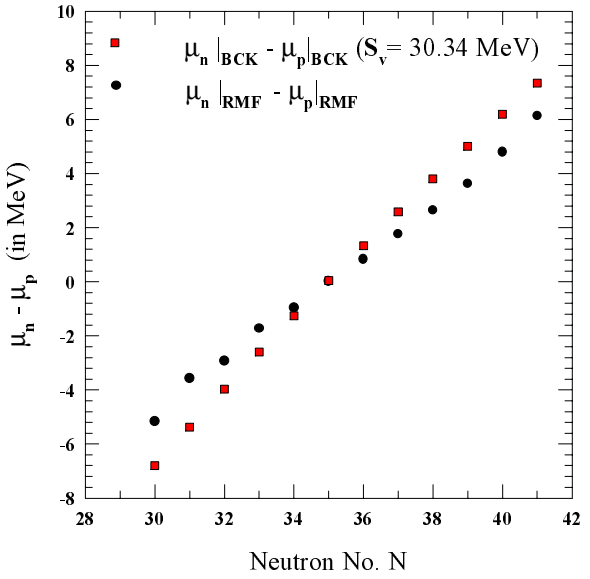

Fig. 6. Difference of proton and neutron chemical potentials $\hat{\mu}|_{RMF}$ (parameter set NL-SH) and $\hat{\mu}|_{BCK}$ for Ni. The BCK-values have been generated from the BCK-EOS using $S_v = 30.34$ MeV, but with the same incompressibility $K = 180$ and $a_v = 16.0$.

4.2. The finite range liquid drop model (FRLDM)

The various forms for the total binding energy of a nucleus W_N that have been quoted in Sect. 2 have all been for spherical nuclei without shell and pairing corrections. A refinement of these simple liquid drop mass formulae of Myers & Swiate-

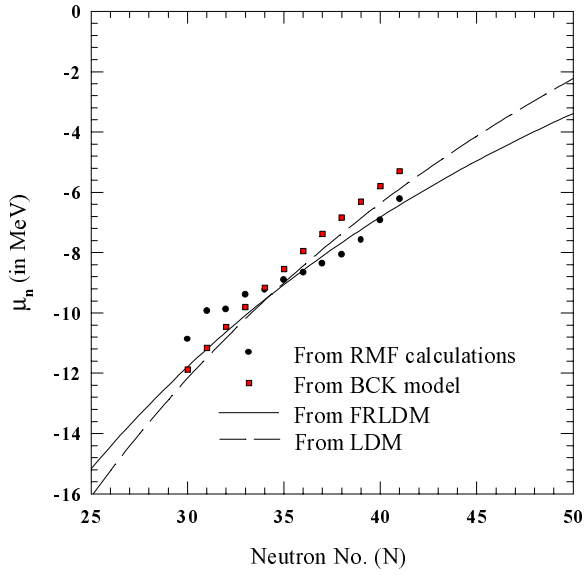

Fig. 7. The chemical potentials $\mu_n|_{RMF}$ and $\mu_n|_{BCK}$, along with the functional forms of the liquid drop model (LDM) given in Eq. (7) and $\mu_n|_{FRLDM}$ discussed in Sect. 4.2 for Ni isotopes. This figure is especially significant because all the Ni isotopes are spherical nuclei.

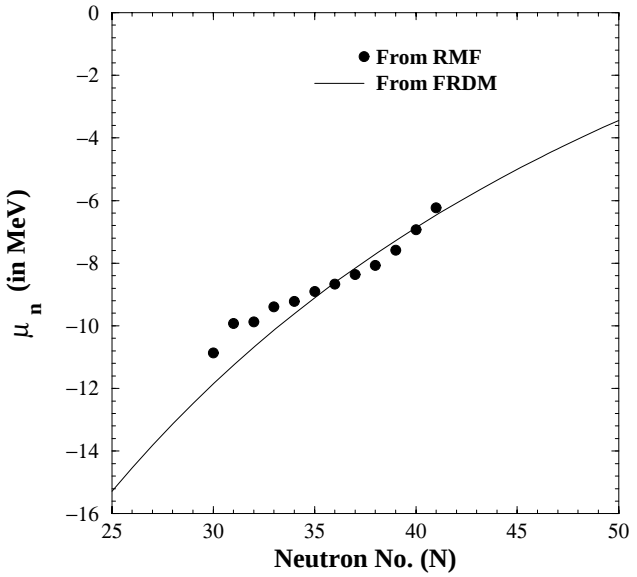

Fig. 8. The chemical potential of neutrons obtained with RMF theory based on the parameter set NL-SH is compared with the functional form of the Finite Range Droplet Model (FRDM) for Ni isotopes.

cki (1966) and Myers et al. (1995) has been made using the microscopic-macroscopic methods. In this approach, the total nuclear potential energy is taken to be the sum of the energy of a term which deals with the bulk properties of nuclear matter and a set of terms which deal with both the shell and pairing effects as well as effects due to nuclear deformation. Here the macroscopic Finite Range Liquid Drop Model FRLDM is used to calculate neutron chemical potentials μ_n in the stellar core for the same range of nuclei for which RMF calculations were made in the previous section. This approach is justifiable for pre-trapping densities where nuclear matter is treated as an ensemble of isolated cold nuclei with a small drip neutron fraction. At higher densities two additional effects would have to be taken into account: (a) the drip neutron contribution as given in Eq. 1 and (b) the lattice corrections made in the Coulomb term. The Finite Range Liquid Drop model is an extension of the LDM of Myers & Swiatecki (1966) with modifications made for the finite range of the nuclear forces by means of a folded Yukawa potential with exponential term.

Recently there has been a further modification of the FRLDM (Myers & Swiatecki 1995) to the FRDM, the Finite Range Droplet Model (Möller et al. 1995). This has been done in order to account, among other things, for the corrections due to Coulomb redistribution effects and the effect of nuclear incompressibility on neutron and proton radii. This improves the predictions of higher moments of nuclear deformation and binding energies in the FRDM model. However, it also depends on a larger number of parameters. Hence, the older FRLDM model is used for in most of our calculations. From Fig. 7 and Fig. 8 we see that these models make practically no differences for the present calculations.

In the FRLDM model, the macroscopic component of the total nuclear binding energy $W_N = W_{mac}(Z,N)$ is given by

$$W_{mac}(Z,N) = -a_v(1-\kappa_v I^2) + a_S(1-\kappa_s I^2)B_1 A^{2/3} + a_o A^0 + c_1 Z^2/A^{1/3} B_3 - c_4 Z^{4/3}/A^{1/3} + f(k_f r_p) Z^2/A - c_a(N-Z) + W\left(|I| + \begin{cases} 1/A & \text{Z=N, odd} \\ 0 & \text{otherwise} \end{cases}\right) + \Delta_{\rm pair},$$

where the average pairing energy $\Delta_{\rm pair}$ is obtained from nuclear binding energies using the 4-point method of Bohr et al. (Sect. 3) and is given by:

$$\Delta_{\rm pair} = \begin{cases} \overline{\Delta}_p + \overline{\Delta}_n - \delta_{np} & \text{Z odd, N odd} \\ \overline{\Delta}_p & \text{Z odd, N even} \\ \overline{\Delta}_n & \text{Z even, N odd} \\ 0 & \text{Z even, N even} \end{cases} \quad (18)$$

where $I = (N-Z)/A$ is the relative neutron-proton excess and $c_1 = \frac{3}{5}\frac{e^2}{r_0}$ and $c_4 = \frac{5}{4}\left(\frac{3}{2\pi}\right)^{2/3} c_1$. The first term $W_{mac}(Z,N)$ is the volume energy, the second the surface energy, with a correction for surface asymmetry, the third term is due to the Coulomb energy, the fifth is the Coulomb exchange term. The other terms are (in that order) due to proton form factor correction to the Coulomb energy, the charge asymmetry energy, and the Wigner term respectively. The numerical values of the various parameters used in this model are quoted in Table 2. The proton form factor correction to the Coulomb energy is given by

$$f(k_f r_p) = -\frac{r_p^2 e^2}{8 r_0^3} \times \left[\frac{145}{48} - \frac{327}{2880}(k_f r_p)^2 + \frac{1527}{1209600}(k_f r_p)^4\right] \quad (19)$$

Both coefficients B_1 and B_3 are shape dependent quantities. The factor B_1 is the relative generalized surface or nuclear energy.

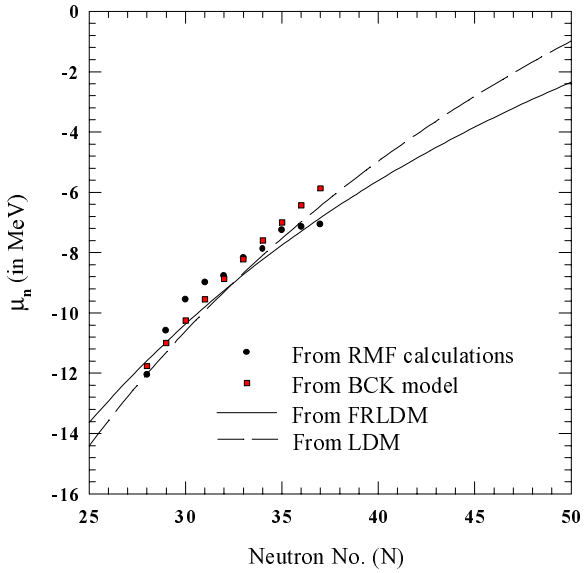

Fig. 9. The chemical potentials $\mu_n|_{RMF}$ and $\mu_n|_{BCK}$, along with the functional forms of the liquid drop model (LDM) given in Eq. (7) and $\mu_n|_{FRLDM}$ discussed in Sect. 4.2 for Fe isotopes.

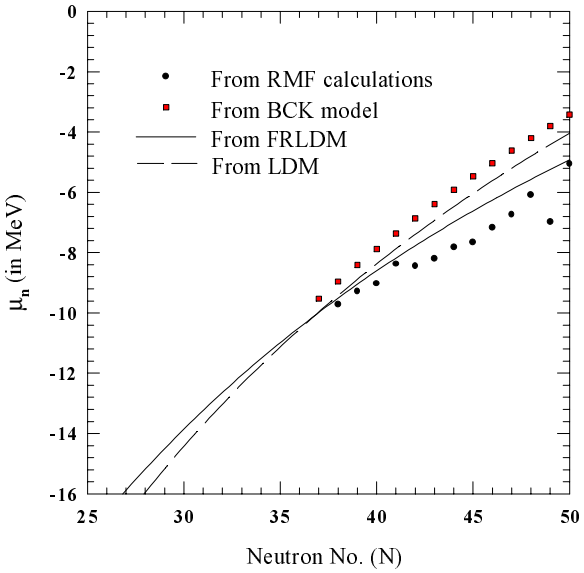

Fig. 10. The chemical potentials $\mu_n|_{RMF}$ and $\mu_n|_{BCK}$, Eq. (7) and $\mu_n|_{FRLDM}$ discussed in Sect. 4.2 for Ga isotopes.

It takes into account the finite range a of the nuclear forces and is given by:

$$B_1 = \frac{A^{-\frac{2}{3}}}{8\pi^2 r_0^2 a^4} \times \int\int_V \left(2 - \frac{|\mathbf{r}-\mathbf{r}'|}{a}\right) \frac{\exp(-|\mathbf{r}-\mathbf{r}'|/a}{|\mathbf{r}-\mathbf{r}'|/a} d^3r d^3r' \quad (20)$$

and B_3 is the relative Coulomb energy and is given by:

$$B_3 = \frac{15A^{-5/3}}{32\pi^2 r_0^5} \times \int\int_V \frac{d^3r d^3r'}{|\mathbf{r}-\mathbf{r}'|} \left[1 - \left(1 + \frac{1}{2}\frac{|\mathbf{r}-\mathbf{r}'|}{a_{den}}\right) \exp(-|\mathbf{r}-\mathbf{r}'|/a_{den})\right] \quad (21)$$

Using Eq. (5), we find the following expression for the volume contribution to μ_n:

$$\mu_n|_{vol} = -16 + 123.04(0.5-x)^2 + 246.08x(0.5-x) \quad (22)$$

Note that the bilinear term in this expression reduces approximately to the linear term in Eq. (7) when symmetric nuclei are considered ($x \simeq 0.5$). The surface etc. contributions to $\mu_n|_{total}$ were obtained by using Eq. (5) on the surface energy, the Coulomb energy and the Coulomb exchange correction components of the FRLDM expression for total energy quoted above. The small corrections due to the shape dependent terms B_1 and B_3 were ignored, as were the other terms in the expression for the total nuclear binding energy.

In Fig. 7 the functional form of μ_n in Eq. (5) using FRLDM is compared with the corresponding RMF values for the spherical Ni isotopes and in Figs. 2, 9, and 10 for the deformed Mn, Fe, and Ga isotopes. It is found that the FRLDM model reproduces the RMF values better than either the BCK-EOS (with the "best" parameters employed by them) or the spherical-LDM results in Eq. (7). A comparison of the binding energy predictions

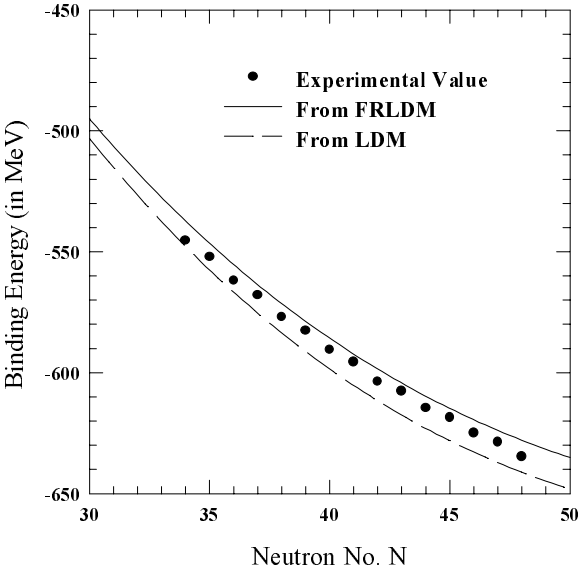

Fig. 11. The nuclear binding energies using the spherical, incompressible LDM, the FRLDM (using volume, surface, coulomb and coulomb exchange terms only) and the experimental values for Ni isotopes.

of both the spherical, incompressible LDM-EOS and FRLDM model is shown in Figs. 11 and 12. The latter models reproduce the binding energies with an accuracy of $\simeq 1$ MeV.

In Fig. 8 we compare the chemical potential of neutrons in the Ni-isotopes calculated within RMF-theory using parameter NL-SH with the results of the Finite Range Droplet Model (FRDM) of Möller et al. (1995).

5. Equation of state at finite temperatures

At low densities, the neutrons, protons and nuclei can be described by an ideal Boltzmann gas. The supernova matter is

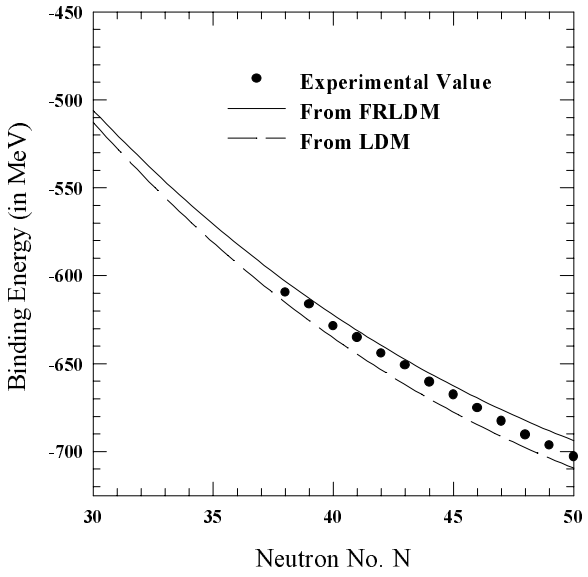

Fig. 12. The nuclear binding energies using the spherical, incompressible LDM, the FRLDM (using volume, surface, coulomb and coulomb exchange terms only) and the experimental values for Ge isotopes.

then in nuclear statistical equilibrium at fixed electron concentration Y_e, where the electrons, positrons and neutrinos (when they are trapped) are non-interacting Fermions (El Eid & Hillebrandt 1980). This approach is justified as long as the nucleon vapor is dilute, i.e. up to about a tenth of the nuclear saturation density. It does not strongly modify the nuclear properties. Higher densities and temperatures require an alternate microscopic description which accounts for interactions between all the nucleons present. Approaches such as equilibrium in the bulk, the compressible liquid drop model, the Thomas-Fermi, or the Hartree-Fock method have been used in the literature.

In the macroscopic approach, the density of a given species is obtained from equations of the Saha-type where one requires partition functions which properly account for the internal excitations of the nuclear species. One also needs the nuclear ground state energies, i.e. the binding energies of these nuclei. Usually one uses semi-empirical mass formulae for the binding energies and Fermi gas based level densities for the nuclear partition functions. The quality of these ingredients determine the level of accuracy of the EOS and its range of applicability. While the macroscopic method may be adequate for the computation of stellar collapse dynamics, one has to take into account shell-effects and pairing correlations in order to calculate threshold Q-values for electron captures on nuclei, if one is interested in the determination of the neutrino spectrum. In addition, ideally one would like to have an approach which is applicable in both low and high density situations encountered in supernova physics. From this point of view a microscopic approach like the RMF method, which satisfies both criteria, is a preferred method. It can also be used to compare results obtained from other microscopic methods.

It can be shown that in the case of low entropy of the stellar core matter, e.g. at the stage of collapse, a multi-phase equilibrium such as between nuclei and nucleonic vapor can be conveniently studied by using a low temperature expansion for the dense nuclei, along with a high temperature expansion for the nucleonic vapor (Vautherin 1994). Vautherin's description of the problem is a mean-field approximation and a simple extension of our RMF calculations to finite temperatures is thus possible.

For a spin saturated, symmetric nucleus (N=Z) the mean field potential from a Skyrme force with a zero range two-body attraction and a three-body repulsion, with coefficients $t_0 = -983.4$ MeV fm^3 and $t_3 = 13105.8$ MeV fm^6 is given by (Ring & Schuck 1980):

$$U(\mathbf{r}) = \frac{3}{4}t_0\rho(\mathbf{r}) + \frac{3}{16}t_3\rho^2(\mathbf{r}). \tag{23}$$

With this potential the single particle orbitals $\phi_i(\mathbf{r})$ are given by the solution of the Schrödinger equation with eigenvalues e_i. The Fermi occupation numbers f_i at finite temperatures are given by $f_i = (1 + \exp((e_i - \mu)/kT))^{-1}$ and the chemical potential μ is fixed from the particle number $\sum_i f_i = A$. This gives the self consistent nucleon density at a finite temperature as $\rho(\mathbf{r}) = \sum_i f_i \left|\phi_i(\mathbf{r})\right|^2$. The entropy of the nucleus obtained in a similar way by the expression for independent fermions:

$$S = -k\sum_i \{f_i \log f_i + (1 - f_i)\log(1 - f_i)\}. \tag{24}$$

For the uniform nuclear matter approximation, the density of the nucleons and kinetic energy densities are found as

$$\rho = g\lambda^{-3}F_{3/2}(\beta U - \alpha) \tag{25}$$

and

$$\tau = 4\pi g\lambda^{-5}F_{5/2}(\beta U - \alpha) \tag{26}$$

where g=4 is the spin and isospin degeneracy factor $(2S + 1)(2I + 1)$, $\lambda = (2\pi\hbar^2/mkT)^{1/2})$ is the thermal wave length, $\beta = 1/kT$, and $\alpha = \beta\mu$. The Fermi-integral F_n is given by:

$$F_n(x) = (2/\sqrt{\pi})\int_0^\infty y^{n-1}(1 + \exp(y + x))^{-1}dy. \tag{27}$$

Once the density and the temperature of stellar matter is specified, the argument $(\beta U - \alpha)$ of the Fermi function is determined, which in turn can be used to compute kinetic energy density, entropy density, pressure, and the free energy density of the system.

A consideration of the phase diagram, i.e. the isothermal lines in $P - \rho$ plane, indicates that at temperatures below a critical temperature a configuration with constant density does not correspond to the lowest value of the free energy for some density ranges. One has a two phase system consisting of a uniform density nucleus and the nucleonic vapor in equilibrium with each other as a more favorable state. Under such conditions, one has:

$$\mu(\rho_N, T) = \mu(\rho_v, T) \quad \text{and} \quad P(\rho_N, T) = P(\rho_v, T). \tag{28}$$

So far, two effects which are important for nuclei have been left out, the finite size (or surface) effects and the Coulomb

interactions. Levit and collaborators (Levit & Bonche 1985; Besprosvany & Levit 1989) have considered the nucleus as a homogeneous system of $A = N + Z$ nucleons inside a spherical volume Ω of radius R which is in equilibrium with the nucleonic vapor of volume Ω_v and density ρ_v. Because of the large incompressibility of nuclear matter it can be shown that the change in the density of the nuclear phase caused by Coulomb and surface tension effects is rather small. Therefore in the equilibrium equations between the nuclear and vapor phases, it is adequate to evaluate the Coulomb and surface terms for the pressure and the chemical potentials at saturation density ρ_0 and $R = R_0 = (3/4\pi\rho_0)^{1/3}$ (Vautherin 1994). Using the Gibbs-Duhem relation $\rho\partial\mu/\partial\rho = \partial P/\partial\rho$ one can also eliminate the density of the nucleus phase in the vapor-nucleus equilibrium equations, and observing that the coefficients of $\rho - \rho_0$ in the expansion of the nuclear pressure and of the chemical potential have to be equal. Thus one has:

$$\mu(\rho_v, T) \;=\; \frac{E_0}{A} - \frac{\pi^2}{4}\frac{(kT)^2}{T_F} + \frac{1}{R_0}\left(\frac{2\alpha(T)}{\rho_0} + \frac{Z^2e^2}{A}\right) \quad (29)$$

The RMF calculations outlined in the previous sections automatically account for the surface and Coulomb effects in the nuclear chemical potential calculations (such as the last term within parentheses in the above equation). Since T_c is quite high, it is adequate to use in the computation of the equation of state at low densities the zero temperature surface tension effects already built into the RMF code for the nuclei, i.e. $\alpha(T) = \alpha(0)$. Therefore the only finite temperature correction is the second term on the RHS of the above equation.

5.1. Lattice size effects

As an attempt to extend the RMF results presented in Sect. 3, to higher densities, the density dependent lattice correction should be incorporated into the Laplace equation for the electric potential:

$$-\Delta A^0(\mathbf{r}) = \rho_p(\mathbf{r}) - \rho_e(\mathbf{r}) \quad (30)$$

where A^0 is the Coulomb potential, $\rho_p(\mathbf{r})$ is the proton charge density and $\rho_e(\mathbf{r})$ is the electron charge distribution density in the Wigner-Seitz cell. Here, the lattice correction has been incorporated into the Coulomb energy part of the total energy by the inclusion of the multiplicative factor $F_{lattice} = (1 - \frac{3}{2}(\frac{\rho}{\rho_s})^{1/3} + \frac{1}{2}(\frac{\rho}{\rho_s}))$ where ρ and ρ_s are the stellar matter and nuclear saturation densities respectively. In Fig. 13 we show the values of $\hat{\mu}$ for Ni isotopes along with the results from Eqs. (7) and (8) for the matter density $\rho = 10^{12}$ g cm^{-3}.

At densities near $\approx 10^{12}$ g cm^{-3} the distance between individual nuclei becomes so short that the nuclear motions begin to be correlated due to the Coulomb interaction between the nuclei and at somewhat higher densities the nuclei arrange themselves on the lattice sites of a crystal. Thus, towards the end of the density regime that one would be interested in for computing early (un-scattered) neutrino spectra, EOS calculations have to take into account screened Coulomb interactions. This is usually

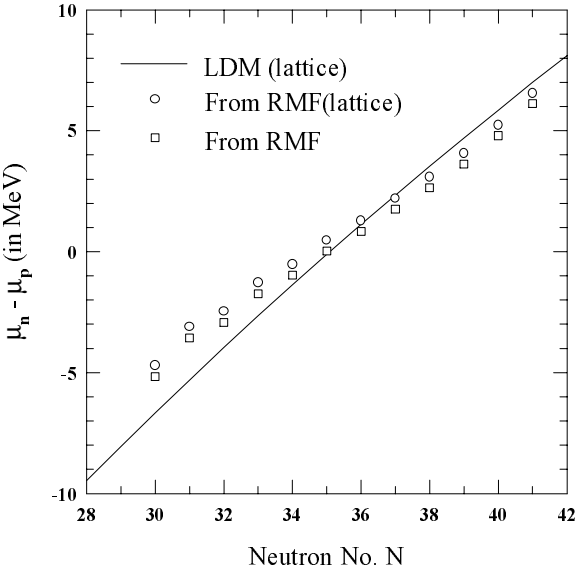

Fig. 13. The difference of neutron and proton chemical potentials ($\hat{\mu} = \mu_n - \mu_p$) for Ni isotopes, taking into account the lattice correction, at a density of 10^{12} g/cm^3. The figure also shows for comparison, the values of $\hat{\mu}|_{RMF}$ without lattice correction, and the (lattice independent) LDM value for $\hat{\mu}$ from Eq. (8).

done by calculating thermodynamic quantities in the Wigner-Seitz approximation. Stellar matter with a plasma parameter $\Gamma = Z^2e^2/RkT \geq 155$, arranges itself in a lattice and the Coulomb interaction energy can be written at zero temperature as:

$$E_c = \frac{3}{5}\frac{Z^2e^2}{R_N}\left\{1 - \frac{3R_N}{2R_c} + \frac{1}{2}\left(\frac{R_N}{R_c}\right)^3\right\} \quad (31)$$

This therefore motivates the inclusion of the density dependent $F_{lattice}$ correction in the RMF equations.

5.2. Asymmetric nuclear matter and approximate solution of the equilibrium equations

To describe nuclei with different neutron and proton numbers as in the neutron-rich situation encountered in the stellar collapse one has to include the bulk asymmetry term $a_\tau x_N^2$ in the mass formula, where $x_N = (N - Z)/A$ is the nuclear asymmetry parameter. By writing the equilibrium equations explicitly in terms of low and high temperature expansions in the nuclear and in the vapor nucleonic chemical potentials, one is able to relate the difference in the nuclear component of the neutron and proton chemical potentials to the asymmetry parameter x_N as:

$$\mu_{Nn} - \mu_{Np} = 4a_\tau(T)x_N, \quad (32)$$

where, $a_\tau(T)$ is the second derivative of the free energy with respect to x_N:

$$a_\tau(T) = \frac{1}{3}T_N - \frac{1}{4}t_0(x_0 + 1/2)\rho_N - \frac{1}{16}t_3\rho_N^2 + \frac{\pi^2}{36}\frac{(kT)^2}{T_N} \quad (33)$$

where $x_0 = 0.48$. Similarly the vapor asymmetry x_v and nuclear asymmetry can be related as:

$$x_v = \tanh(2a_\tau x_N/kT), \tag{34}$$

while the vapor density can be related to the average nuclear chemical potential $\mu_N = (\mu_{Nn} + \mu_{Np})/2$:

$$\rho_v = g\lambda^{-3}(1-x_v^2)^{-1/2} exp(\mu_N/kT). \tag{35}$$

Here μ_N defined above can be approximated to the first order in x_N as:

$$\mu_N = \frac{E_0}{A} + \frac{1}{9}\frac{\rho_N - \rho_0}{\rho_0}\left(K - \frac{5\pi^2(kT)^2}{2T_F}\right) - \frac{\pi^2(kT)^2}{12T_F}. \tag{36}$$

It has been shown (Vautherin 1994) that it is a good approximation to replace a_τ by its value at zero temperature and normal density, since the dependence of a_τ on temperature is weak. The pressure in the vapor phase is given by the high temperature approximation:

$$\begin{aligned} P_v \;=\; & \rho_v T\left(1 + \frac{\rho_v\lambda^3}{4g\sqrt{2}}(1+x_v^2) + \cdots\right) \\ & + \frac{1}{8}t_0\rho_v^2(3 - x_v^2(2x_0+1)) + \frac{1}{8}t_3\rho_v^3(1-x_v^2). \end{aligned} \tag{37}$$

Although the total pressure is dominated by the lepton pressure, one may estimate the nucleonic component from the above expression.

6. Summary

Using the relativistic mean field method, we have evaluated in this paper properties of individual nuclear species which play a significant role for the physical and thermodynamic properties as well as the dynamics of a pre-supernova collapsing stellar core. In particular, we have determined the nuclear chemical potentials μ_n and μ_p, which, along with the nuclear weak interaction strengths control the neutronization of the matter. We have focussed our interest on properties of nuclei present in the core at a density range 10^9 to 10^{12} g/cm^3 which corresponds to the temperature range of $\simeq 0.2$ to 1.5 MeV. In this range the core composition is dominated by heavy, neutron-rich, $f-p$ shell nuclei in a Saha equilibrium, with a low density vapor of free neutrons, and an even lower density vapor of free protons. In this temperature and density range, matter can be treated as an ensemble of non-interacting Boltzmann particles, at least at $\rho_{10} = 0.1 \;-\; 100\; g/cm^3$. This implies that nuclear properties under these conditions are determined by those of individual nuclei, and structure effects like shell effects, pairing and deformation play a significant role.

Our study has been motivated by the fact that the existing equations of state used for numerical studies of stellar core collapse are based on macroscopic liquid-drop models, which generally do not take into account shell, pairing and other nuclear structure effects - which play an important role at lower energies. These EOS are suitable for matter at $T \gg 1.5$ MeV, and $\rho \gg 10^{12}$ g/cm^3, when the nuclear matter undergoes a phase transition from the state where individual nuclei are present in a gas of dripped nucleons, to the state where the nuclei merge into infinite nuclear matter (see Sect. 1 and (BBAL, BBCW, Cooperstein (1985)). Because shell and pairing effects are already washed out at temperatures beyond 1 MeV and at densities beyond trapping density i.e. 10^{12} g/cm^3, ideally, a low-density, zero temperature EOS would be desirable, which smoothly goes over to the high density, high temperature equations of state based on the liquid drop model (see Swesty et al. 1994).

In order to account for the shell and pairing effects persistent at low temperatures we studied the nuclear structure effects in the framework of relativistic mean field theory, using a Lagrangian with non-linear self-interactions for the σ-meson. This method has been shown to provide a good description of the ground state properties of nuclei (Gambhir et al. 1990). The nuclei of interest range from ^{54}Mn$_{25}$ to ^{81}Ge$_{32}$ (see Tables 3, 4, 5, and 6), predominantly neutron-rich $f-p$ shell nuclei. It is the first time that the RMF method is used to calculate the binding energies of nuclei with a neutron excess in the range of interest.

In order to test the validity of high-density equations of state at low densities BBAL we compare the chemical potentials μ_n and $\hat{\mu}$ with those obtained in RMF theory and we find considerable deviations. To study the influence of nuclear compressibility we have also compared the chemical potentials $\mu_n|_{RMF}$ and $\mu_p|_{RMF}$ with those of the compressible liquid-drop model based on the EOS of BCK. To test the effects of a variation in the nuclear incompressibility K_0 and in the volume symmetry energy S_v, we computed the results of BCK with a range of values of K_0 and S_v. We find that the results are more sensitive to the variation in S_v than in K_0. From a fit of $\hat{\mu}|_{RMF}$ to the analytical expression for $\hat{\mu}|_{BCK}$, we find an "averaged" value of S_v of 30.34. Further, to account for nuclear deformation effects we use the FRLDM expression for the nuclear binding energy to compute μ_n and $\hat{\mu}$. A comparison of RMF values with this "extended" macroscopic model demonstrates the influence of shell and pairing effects on μ_n and on $\hat{\mu}$ (see Figs. 11 and 12).

Finally, in order to take into account the first order Coulomb correlations between the nuclei at high densities, we include a lattice correction in our RMF computations of $\hat{\mu}$. A comparison of these lattice corrected RMF results with the BBAL/Fuller EOS for $\hat{\mu}$ is shown in Fig. 13. We have also outlined the reasons for obtaining the relatively small corrections that are needed for finite temperature corrections to the EOS at low entropies relevant for the early stages of a massive star's core collapse. Methods to generalize the results to finite temperature EOS calculations, using the chemical potentials and other quantities obtained from RMF calculations have been indicated.

Many groups have computed and analysed the collapse of the stellar core of a massive star to evaluate the effects of various physical processes in determining conditions prior to core-bounce. As collapse is shown to be a nearly homologous one (see BBAL and references therein), a one-zone collapse is adequate for the investigation of thermodynamic and nuclear properties (see e.g. EH (1980); Hillebrandt et al. (1984) which used the EOS of Wolff & Hillebrandt (1983); Ray et al. (1984); Fuller

Table 8. Comparison of the nucleonic chemical potentials for RMF and El Eid & Hillebrandt EOS in stellar collapse using data for a star of initial mass $15M_{\odot}$.

Model	ρ_{10}	Y_e	Mean Nucleus	μ_n (MeV)	μ_p (MeV)
RMF	0.37	0.42	68	-6.93	-11.7
EH	0.37	0.42	52	-7.08	-11.5

(1982); etc). The EOS of dense stellar matter affects the electron capture rate and the evolution of the lepton fraction mainly through the influence of the chemical potentials of the free nucleons (see Murphy (1980); Sutaria & Ray (1997)). For example, the thermodynamic quantities at the beginning of stellar collapse for the RMF results and those of EH are compared in Table 8. However, the intrinsic electron capture rates on nuclei employed by different authors have been different and have evolved considerably over the years. It is therefore difficult to extract the purely EOS related effects on neutronisation of different calculations. The stellar collapse calculation using the full RMF EOS in a self-consistent manner with the latest electron capture rates is in preparation and the details of the evolution of nuclear and thermodynamic variables will be published elsewhere.

Acknowledgements. This research is part of the 9th Five Year Plan project 9P-208[a] at Tata Institute of Fundamental Research. AR was a U.S. National Research Council Senior Research Associate during part of the time when this research was carried out. Part of the work has been supported by the Bundesministerium für Bildung und Forschung under the contract 06 TM 875.

References

Baron E., Cooperstein J., Kahana S., 1985, Nucl. Phys. A440, 744
Baym G., Bethe H.A., Pethick C.J., 1971a, Nucl. Phys. A175, 225
Baym G., Pethick C.J., Sutherland P.G., 1971b, ApJ 170, 299
Bethe H.A., Brown G.E., Applegate J., Lattimer J. M., 1979, Nucl. Phys. A324, 487
Bethe H.A., Brown G.E., Cooperstein J., Wilson J.R., 1983, Nucl. Phys. A403, 625
Besprosvany J., Levit S., 1989, Phys. Lett. 217B, 1
Bonche P., Vautherin D., 1981, Nucl. Phys. A372, 496
Boguta J., Bodmer A.R., 1977, Nucl. Phys. A292, 413
Bohr A., Mottelson B. R., 1969, Nuclear Structure I, W.A. Benjamin Publishers
Cooperstein J., Baron E., 1990, In: Petschek A.G. (ed.) Supernova. Springer-Verlag, p. 213
Cooperstein J., 1985, Nucl. Phys. A438, 722
El Eid M.F., Hillebrandt W., 1980, A&AS 42, 215
Fuller G.M., 1982, ApJ 252, 741
Gambhir Y.K., Ring P., Thimet A., 1990, Ann. Phys. 198, 132
Haensel P., Zdunik J. L., Dobaczewski J., 1989, A&A 22, 353
Hillebrandt W.H., Nomoto K., Wolff R., 1984, A&A 133, 175
Hillebrandt W.H., 1994, In: Bludman S., Mochkovich R., Zinn-Justin J. (eds.) Supernovae. Les Houches Session LIV,, Elsevier
Hix W.R., Thielemann F.-K., 1996, ApJ 460, 869
Lalazissis G.A., König J., Ring P., 1997, Phys. Rev. C55, 540
Lamb D.Q., Lattimer J.M., Pethick C.J., Ravenhall D.G., 1978, Phys. Rev. Lett. 41, 1623
Lamb D.Q., Lattimer J.M., Pethick C.J., Ravenhall D.G., 1983, Nucl. Phys. A411, 449
Lattimer J.M., Pethick C.J., Ravenhall D.G., Lamb D.Q., 1985, Nucl. Phys. A432, 646
Levit S., Bonche P., 1985, Nucl. Phys. A347, 426
Möller P., Nix J.R., Myers W.D., Swiatecki W.J., 1995, At. Data and Nucl. Data Tables 59, 185
Murphy M., 1980, ApJS 42, 385
Myers W.D., Światecki W.J., 1966, Nucl. Phys. 81, 1
Myers W.D., Światecki W.J., 1995, Nucl. Phys. A587, 92
Nadjakov E.G., Marinova K.P., Gangrsky Yu.P., 1994, At. Data and Nucl. Data Tables 56, 133r
Negele J.W., Vautherin D., 1973, Nucl. Phys. A207, 298
Pethick C.J., Ravenhall D.G., 1995, Ann. Rev. Nucl. Part. Sci. 45, 429
Ravenhall D.G., Bennet C.D., Pethick C.J., 1972, Phys. Rev. Lett. 28, 978
Ray A., Chitre S.M., Kar K., 1984, ApJ 285, 766
Ray A., Sutaria F.K., Sheikh J.A., 1999, In: Phillips M.M., Suntzef N. (eds.) Supernova 1987A: Ten Years Later. Astron. Soc. Pacific Ser., in press
Reinhard P.-G., Rufa M., Maruhn J., Greiner W., Friedrich J., 1986, Z. Phys. A323, 13
Ring P., Schuck P., 1980, The Nuclear Many-body Problem. Springer Verlag, New York
Serot B.D., Walecka J.D., 1986, Adv. Nucl. Phys. 16, 1
Sharma M.M., Nagrajan M.A., Ring P., 1993, Phys. Lett. B312, 377
Sheikh J.A., Maharana J.P., Gambhir Y.K., 1993, Phys. Rev. C48, 192
Sutaria F.K., 1997a, Ph.D. Thesis, Mumbai University
Sutaria F.K., Ray A., 1997, Phys. Rev. Lett. 79, 1599
Sutaria F.K., Sheikh J.A., Ray A., 1997b, Nucl. Phys. A621, 375c
Swesty F.D., Lattimer J.M., Myra E.S., 1994, ApJ 425, 195
von Groote H., Hilf E.R., Takahashi K., 1976, At. Data Nucl. Data Tables 17, 418
Vautherin D., 1994, In: Bludman S., Mochkovitch R., Zinn-Justin J. (eds.) Supernova. Les Houches Session LIV
Wolff, R. G., Hillebrandt, W., 1983, In: Arnett, Truran (eds.) Nucleosynthesis. Univ of Chicago Press, p. 131